Title
CHROMATOGRAPHIC TRANSPORT OF ALKALINE BUFFERS THROUGH RESERVOIR ROCK

Authors
Jensen, J.A.
Radke, C.J.

Publication Date
1985-09-01

Lawrence Berkeley Laboratory
UNIVERSITY OF CALIFORNIA

EARTH SCIENCES DIVISION

Presented at the 60th Annual Fall Technical
Conference of SPE, Las Vegas, NV,
September 22-25, 1985

CHROMATOGRAPHIC TRANSPORT OF ALKALINE BUFFERS
THROUGH RESERVOIR ROCK

J.A. Jensen and C.J. Radke

September 1985

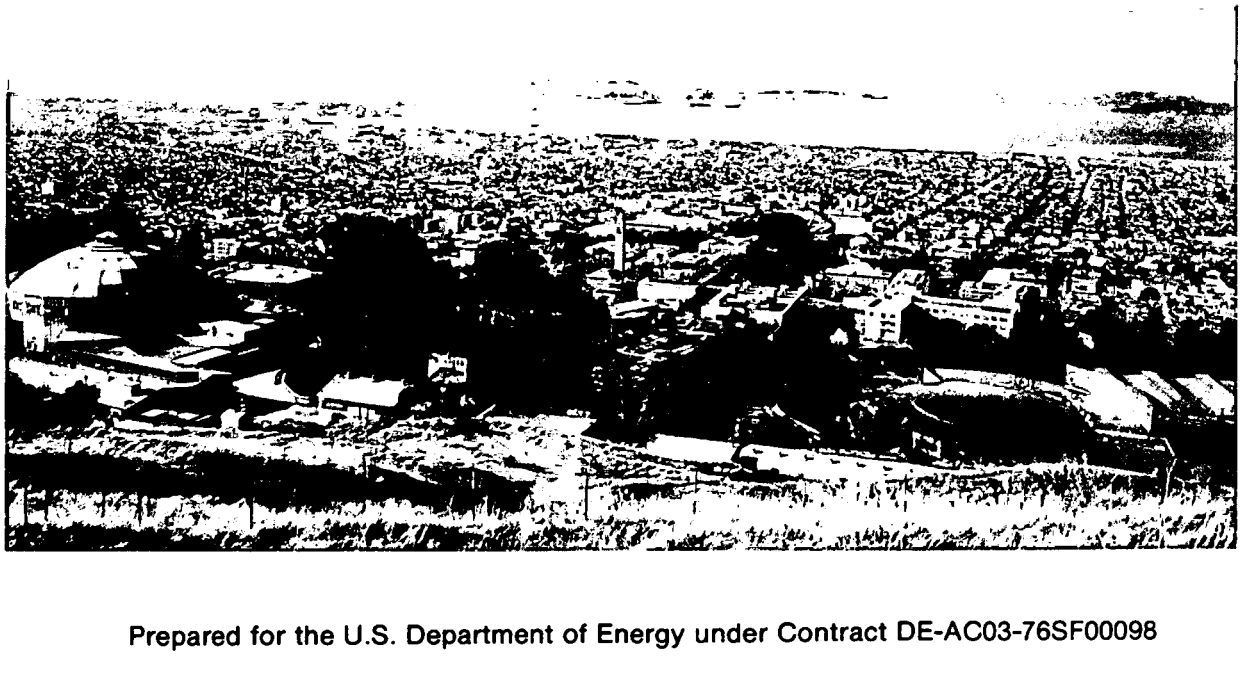

Prepared for the U.S. Department of Energy under Contract DE-AC03-76SF00098

DISCLAIMER

LBL-19999

Chromatographic Transport of Alkaline Buffers Through Reservoir Rock

by

J.A. Jensen

Chemical Engineering Department
University of California
Berkeley, California 94720

C.J. Radke

Earth Sciences Division
Lawrence Berkeley Laboratory
and
Chemical Engineering Department
University of California
Berkeley, California 94720

September 1985

For presentation at the

60th Annual Fall Technical Conference of SPE

September 22-25, 1985

Las Vegas, Nevada

SPE 14295

Chromatographic Transport of Alkaline Buffers Through Reservoir Rock†

by

J.A. Jensen and C.J. Radke
Chemical Engineering Department
University of California
Berkeley, California 94720

ABSTRACT

Use of relatively low-pH alkaline buffers, such as sodium carbonate or sodium silicate, is explored as a means for overcoming sodium/hydrogen ion-exchange delay in alkaline waterflooding. A local equilibrium chromatographic model is outlined to describe the concentration velocities for injection of alkaline buffers into a linear porous medium which exhibits reversible sodium/hydrogen exchange. The theory predicts a buffer ion-exchange wave which is indeed substantially faster than that for equivalent-pH sodium hydroxide solutions.

New experimental displacement data are presented for NaOH over a pH range from 11 to 13 and for 0.1, 0.5, and 1.0 w/o Na_2CO_3 flowing through a 1 w/o NaCl brine saturated Berea sandstone core at 50°C. To permit a complete description of the system, column effluent concentrations are measured for sodium ions, hydroxide ions, ^3HOH-tagged water, and ^{14}C-tagged carbonate. The experiments confirm that Na_2CO_3 propagates through the Berea sand at a higher rate than NaOH. For example, at pH = 11.4 Na_2CO_3 migrates with a velocity that is 3.5 times faster than NaOH.

---

†References and illustrations at end of paper.

Comparison of experiment with the ion-exchange chromatography theory shows good agreement. We successfully model the concentration histories of tritium-labelled water, total carbon, sodium, and hydroxide, all with no adjustable parameters.

This work establishes with both theory and experiment that buffered alkali significantly increases the propagation speed of hydroxide in reservoir sands in comparison with unbuffered alkali at equivalent sodium and hydroxide concentrations. Since lower pH buffered alkali can also protect against rock dissolution loss, the validated reduction of buffer ion-exchange lag considerably improves the promise of the alkaline-flooding process for field application.

INTRODUCTION

Early work on alkaline waterflooding focused almost entirely on dilute bases with no other chemical additives [1], even though the acidic crude oils were relatively viscous and the typical acid numbers did not permit generation of large surfactant amounts. Both laboratory and field recoveries have, accordingly, not been encouraging. Recently, however, in combination with dilute cosurfactants [2,3] and mobility control [3,4] excellent tertiary recovery efficiencies are found in laboratory alkaline displacement studies, even at pH levels down to 11 [4]. Field application of these augmented processes is questionable because laboratory core results may not properly address the question of rock reaction loss.

Alkali rock loss can be divided into bulk mineral dissolution and surface mineral ion exchange [5-11]. Rock dissolution reactions are generally slow

and difficult to quantify in laboratory time scales, while rock ion-exchange reactions are generally fast and reversible. This paper addresses the use of alkaline buffers to overpower the reversible ion-exchange reactions.

Figure 4 of reference [8] displays the importance to oil recovery of the reversible alkali-rock exchange reaction. That is, dilute caustic transports much slower than the frontal advance rate thereby delaying oil recovery rates [12]. For example, according to Figure 4 of reference [8], a pH = 11 caustic solution does not appear in the effluent of an argillaceous Wilmington sand until after 12 PV.

The origin of caustic chromatographic delay is sodium/hydrogen ion exchange which obeys the following generic reaction:

$$\bar{M}H + Na^+ + OH^- \overset{K_I}{\underset{+}{\rightleftharpoons}} \bar{M}Na + H_2O \ , \qquad (1)$$

where $\bar{M}$ denotes a mineral exchange site [6,8,12-14]. In flowing through a reservoir rock, sodium ions must "fill" the available exchange sites before they can progress downstream. This retards the alkali according to Eqn. (1).

One obvious means for overpowering the ion-exchange delay of caustic is to increase the bulk solution concentration relative to the exchange site density [8,12]. However, for most reservoir minerals, higher pH levels favor higher solubilities and kinetic rates leading to more extensive rock dissolution [8,15,16]. It may be wise to pursue alkaline waterflooding at as low a pH as possible, only sufficient to activate the oil-soluble, acid surfactant precursors. Unfortunately, in reservoir time scales low concentrations of NaOH (e.g., pH ~ 10.5 to 11.5) are rapidly depleted to ineffective levels [8].

To mitigate against alkali consumption and still operate in the lower pH ranges we investigate the use of alkaline buffers, such as sodium carbonate or sodium silicate. Specifically, this paper attacks the problem of reducing

sodium/hydrogen ion exchange delay. Qualitatively, it is straightforward to understand the role of a buffer in ion exchange chromatography. Consider the carbonate/bicarbonate equilibrium reaction:

$$CO_3^{=} + H_2O \overset{K_1}{\underset{}{\rightleftharpoons}} HCO_3^{-} + OH^{-}, \qquad (2)$$

which will buffer within 1 or 2 pH units of $p(K_w/K_1) = 10.25$ at 25°C [17] where K_1 is the equilibrium constant of Eqn. (2) and K_w is the dissociation constant of water. As an alkaline carbonate solution transports through a reservoir sand, sodium/hydrogen ion exchange occurs to delay hydroxide according to Eqn. (1). Concurrently, bicarbonate ions are formed following Eqn. (2) to replenish the hydroxide lost to ion exchange. In this manner hydroxide is carried downstream more quickly (i.e., the hydroxide concentration velocity is increased).

Similar reasoning can be applied to the silicate buffer system with the solution equilibrium reaction:

$$H_2SiO_4^{=} + H_2O \overset{K_3}{\underset{}{\rightleftharpoons}} H_3SiO_4^{-} + OH^{-}, \qquad (3)$$

which buffers around $p(K_w/K_3) = 13$ at 25°C [8,15,16,18]. Indeed, any buffering alkali could apply, differing only on the dissolvable concentration levels and on the pH at which buffering occurs.

Our goal is to quantify the above reasoning in a chromatographic model of buffering systems. Essentially, we seek a theory of equilibrium ion-exchange chromatography with solution complexation [19,20]. The theory is presented in the next section. Comparison to experimental data then follows.

ALKALINE BUFFER CHROMATOGRAPHY

We treat in detail only the sodium carbonate case. Other buffer systems follow by analogy. Before outlining the transport theory, it is necessary to review the solution and ion-exchange equilibrium restrictions.

Equilibrium Chemistry

In an aqueous carbonate/brine solution Eqn. (2) applies along with protonation of the bicarbonate:

$$HCO_3^- + H_2O \overset{K_2}{\rightleftharpoons} H_2CO_3 + OH^- , \tag{4}$$

where K_2 is the designated equilibrium constant (values for all the equilibrium speciation constants used in this work are listed in Table 1). In Eqn. (4) H_2CO_3 indicates the aqueous concentration of dissolved carbon dioxide. Of course, dissociation of water takes place:

$$H_2O \overset{K_w}{\rightleftharpoons} H^+ + OH^-, \tag{5}$$

and the aqueous phase must be electrically neutral:

$$C_{Na} + C_H = C_{OH} + C_{HCO_3} + 2C_{CO_3} + C_{Cl}, \tag{6}$$

where C_i represents the bulk molar concentration of species i. Later we also use brackets, [ ], to denote bulk molar concentrations.

At the aqueous solution/mineral surfaces, the mass-action form of Eqn. (1) together with conservation of exchange sites specifies the sodium/hydrogen exchange isotherm [14]:

$$\frac{n_{Na}}{n_{max}} = \frac{K_I C_{Na} C_{OH}}{1 + K_I C_{Na} C_{OH}} , \tag{7}$$

where K_I is the overall exchange equilibrium constant having units of $m^6/kmol^2$, n_{Na} is the moles of sodium occupied sites per unit mass of solid rock, and n_{max} is the total exchange site density or the hydrogen exchange capacity, again in units of mol/g of solids. Eqn. (7) is reminiscent of a Langmuir isotherm [21,22]. It is not identical to the Langmuir formula because the surface-exchange uptake of sodium (or hydroxide) is a function of both sodium and hydroxide ion concentrations. That is, the number of sites in the sodium form can be augmented either by increasing the brine concentration at fixed pH or by increasing the hydroxide level in a fixed sodium background. The quantitative behavior of Eqn. (7) is crucial to the chromatography calculations presented below.

Chromatography

We impose the standard restrictions of an isothermal, homogeneous, linear porous medium with completely exposed surface exchange sites so that local equilibrium applies [12,19,23,24]. The core is water saturated and all chemical species are dilute, exhibiting no volume changes upon mixing. Most importantly, we neglect axial dispersion so that only mass-average breakthrough times are predicted, not the entire shape of the concentration histories about their mean elution times [19, 22-24]. Finally, the initial solution composition in the column is uniform and a step increase in alkali concentration is imposed at the inlet. This is sometimes called the constant presaturation-constant feed case.

In a Na_2CO_3/NaCl solution there are seven molecular species: Na^+, H^+, OH^-, Cl^-, $CO_3^=$, HCO_3^-, and H_2CO_3. The equilibrium relations of Eqns. (2), (4), (5), and electroneutrality in Eqn. (6) demand that only three are

independent. Chloride ions, total carbon content, and sodium ions is the most cogent choice. The concentration of all remaining species can be expressed in terms of these three.

Chloride Conservation

Conservation of the nonadsorbing anionic chloride species reads in light of the nondispersive assumption:

$$\frac{\partial C_{Cl}}{\partial \tilde{t}} + \frac{\partial C_{Cl}}{\partial \tilde{z}} = 0 \ , \tag{8}$$

where $\tilde{t} = ut/\phi L$ is a dimensionless time or PV throughput with u the superficial velocity, t the time, ϕ the bed porosity, and L the bed length. $\tilde{z} = z/L$ is the dimensionless axial bed distance. For a step-concentration change the solution to Eqn. (8) is a dimensionless unit-velocity chloride concentration wave [22-25] or

$$\tilde{z}/\tilde{t} = 1 \ . \tag{9}$$

Thus, a chloride or salinity wave progresses at the reduced frontal advance rate, as sketched on the $\tilde{z}$-$\tilde{t}$ diagram of Fig. 1. Ahead of the salinity wave, in Region I, the chloride concentration is at the initial column level while behind that wave, in Regions II and III, the chloride concentration is set by the feed value.

Total Carbon Conservation

It is convenient to define a total carbon concentration by atom balance:

$$C_{TC} = C_{CO_3} + C_{HCO_3} + C_{H_2CO_3} \tag{10}$$

None of the molecular forms of the carbonate are presumed to interact with the mineral surfaces. Further, solution compositions considered here do not exceed the aqueous solubility of CO_2. Then, conservation of total carbon in the column reads

$$\frac{\partial C_{TC}}{\partial \tilde{t}} + \frac{\partial C_{TC}}{\partial \tilde{z}} = 0 \, . \tag{11}$$

The mathematical solution of Eqn. (11) is identical to that of Eqn. (8): a total carbon shock wave of unit reduced velocity propagates down the column, as described by Eqn. (9) and demonstrated in Fig. 1. In Region I of Fig. 1, the total carbon concentration is at the initial column value. Here it is set to zero. Upstream of the total carbon wave, in Regions II and III of Fig. 1, the three carbonate species redistribute. Sodium conservation prescribes this species distribution. Nevertheless, Eqn. (11) demands that the total carbon concentration in Regions II and III remains constant at its injection amount.

Sodium Conservation

Since sodium ions exchange with the reservoir sand, their conservation statement includes an adsorption rate term, $\partial n_{Na}/\partial \tilde{t}$:

$$\frac{\partial C_{Na}}{\partial \tilde{t}} + \frac{\rho_s(1-\phi)}{\phi} \frac{\partial n_{Na}}{\partial \tilde{t}} + \frac{\partial C_{Na}}{\partial \tilde{z}} = 0 \, , \tag{12}$$

where ρ_s is the solid rock density. For local equilibrium Eqn. (1) states that the sodium uptake is a dual function of the bulk solution sodium and hydroxide concentrations or

$$\frac{\partial n_{Na}}{\partial \tilde{t}} = \frac{\partial n_{Na}}{\partial C_{Na}} \frac{\partial C_{Na}}{\partial \tilde{t}} + \frac{\partial n_{Na}}{\partial C_{OH}} \frac{\partial C_{OH}}{\partial \tilde{t}} \, . \tag{13}$$

Since hydroxide is not a chosen independent species, it must be eliminated from Eqn. (13). To do this, let f denote the functionality between the hydroxide concentration and the three independent species concentrations of chloride, total carbon, and sodium:

$$C_{OH} = f(C_{Na}, C_{Cl}, C_{TC}) \cdot \tag{14}$$

f is established by solving simultaneously the mass-action expressions for Eqns. (2), (4), and (5) with electroneutrality in Eqn. (6) and with the definition of total carbon concentration in Eqn. (10). An exact form for f is listed in Eqn. (A1) of the appendix.

Upstream of the total carbon-salinity wave Eqns. (8) and (11), and Fig. 1 illustrate that $\partial C_{Cl}/\partial \tilde{t} = \partial C_{TC}/\partial \tilde{t} = 0$. With this simplification Eqns. (12) - (14) combine to give the desired result:

$$\left\{1 + \rho_s \frac{(1-\phi)}{\phi} \left[\frac{\partial n_{Na}}{\partial C_{Na}} + \frac{\partial n_{Na}}{\partial C_{OH}} \frac{\partial f}{\partial C_{Na}}\right]\right\} \frac{\partial C_{Na}}{\partial \tilde{t}} + \frac{\partial C_{Na}}{\partial \tilde{z}} = 0 \cdot \tag{15}$$

Characteristics applied to Eqn. (15) states that the concentration velocities of the sodium ions, $d\tilde{z}/d\tilde{t}$, are expressed by [22]:

$$\frac{d\tilde{z}}{d\tilde{t}} = \left[1 + \frac{\rho_s(1-\phi)}{\phi} \left(\frac{\partial n_{Na}}{\partial C_{Na}} + \frac{\partial n_{Na}}{\partial C_{OH}} \frac{\partial f}{\partial C_{Na}}\right)\right]^{-1} \cdot \tag{16}$$

The right side of Eqn. (16) is an increasing function of sodium ion concentration [26]. That is, the ion-exchange isotherm is "favorable" or convex to the ordinate. The result is that higher sodium ion concentrations travel at faster concentration velocities. Upon a step increase in C_{Na} at the column face, an ion-exchange shock wave will commence [22-25].

Aris and Amundson [22] show by material balance that the velocity of this ion-exchange shock wave is retarded or

$$\tilde{z}/\tilde{t} = \left[1 + \rho_s \frac{(1-\phi)}{\phi} \frac{\Delta n_{Na}}{\Delta C_{Na}}\right]^{-1}, \qquad (17)$$

where the ratio $\Delta n_{Na}/\Delta C_{Na}$ is the slope of the exchange-isotherm chord connecting the concentration states at the rear and front of the shock wave. Eqn. (17) is general in the sense that it is valid for any shock occuring in the column. In particular, it applies at the salinity and total carbon waves. Since the salinity and total carbon waves have unit concentration velocities, we discover in this situation that

$$\Delta n_{Na} = 0, \text{ for salinity and/or total carbon waves} . \qquad (18)$$

Thus, the adsorption of sodium ions must be identical at the front and rear of the salinity and total carbon waves.

The complete mathematical solution may now be summarized and displayed in Fig. 1. Three regions are evident. Region I corresponds to the presaturation solution composition. Region III reflects the constant injection solution composition. An intermediate plateau composition emerges in Region II. In between these three regions two shock waves arise: the coincident salinity and total carbon waves and the ion-exchange wave.

First, the unit-velocity, salinity-total carbon wave penetrates into the column. Across this wave $\Delta n_{Na} = 0$, as demanded by Eqn. (18). Since the presaturation concentrations are known, the composition of the intermediate plateau region is calculated to satisfy the bulk solution equilibria of Eqns. (2), (4) - (6), and (10), along with no adsorption change of sodium ions. Once the intermediate-plateau concentrations are found, the velocity of the alkali ion-exchange wave follows from Eqn. (17), since the injection solution

composition is pre-set. This completes the numerical calculation. Considerable details on the calculation scheme are available in the thesis of Jensen [26].

Application of the theory to the Na_4SiO_4/NaCl system is by direct analogy. The companion deprotonation reaction to Eqn. (3) is invoked:

$$H_3SiO_4^- + H_2O \overset{K_4}{\rightleftharpoons} H_4SiO_4 + OH^-, \tag{19}$$

and a total silicon balance replaces Eqn. (11). The NaOH/NaCl case immediately emerges from the carbonate chromatographic theory when all carbonate species concentrations are nulled.

Sodium Carbonate and Sodium Hydroxide Concentration Histories

Fig. 2 shows a calculated history on a semilogarithmic scale for injecting 1 w/o Na_2CO_3 (pH_I = 11.6) in 1 w/o NaCl into a reservoir sand initially at pH_o = 8 also in 1 w/o brine. The equilibrium constants for the carbonate hydrolyses are taken from Table 1. Reasonable values for the sodium/hydrogen ion-exchange parameters are $K_I = 10^6$ N^{-2} and n_{max} = 0.85 mequiv/100g [8,12,14]. In this figure, and those to follow, the subscript o refers to the initial column state, while the subscript i refers to the column inlet.

Since the NaCl background concentration is unaltered, no salinity wave appears. The total carbon wave elutes at 1 PV with a total carbon concentration of 9.5 (10^{-2}) N. Intermediate-plateau hydroxide level is pH = 7.8 and the plateau sodium concentration lies between the initial and inlet levels. Carbonate speciation is noted in the figure. Alkali breaks through at $\tilde{t}_b$ = 1.74 PV with the ion-exchange wave.

Comparison between the carbonate buffer and caustic is provided in Fig. 3 at identical pH_i (= 11.6) and brine content. In this figure, only an alkaline ion-exchange wave exists, which elutes at $\tilde{t}_b$ = 12.4 PV . Theory predicts a dramatic enhancement of the ion-exchange wave velocity for the carbonate buffer relative to dilute caustic.

To provide a quantitative test of the buffer chromatography model, experiments are required in which the ion-exchange constants K_I and n_{max} are known beforehand. In the column experiments, which are discussed next, we seek additionally to verify the intermediate plateau and to ascertain that total carbon behaves as a noninteracting tracer.

EXPERIMENT

Standard dynamic column displacements are performed on a single, unfired, vacuum-saturated Berea core at 50°C and at a typical frontal advance rate of 0.7 mm/s (194 ft/day). Two precision liquid chromatography pumps (Waters, 6000A) supply continuously 1 w/o NaCl brine presaturation solution and an alkaline solution under study to a low dead-volume sample injection value (Valco, 6-port) which is affixed directly to the core inlet. At least 100 PV of brine are flushed through the column prior to switching the injection valve to the alkaline solution. After the thorough brine preflushing, the effluent pH reaches a constant value of approximately 9.4 (the difference between the effluent and influent pH values is possibly due to the dissolution of carbonates in the sandstone matrix). During the alkaline displacements, 0.05 PV incremental samples are collected automatically. The fraction collector (LKB 2/12 Redirac) is housed in a subatmostpheric, hooded chamber as required when using volatile radioisotropes. Each sample is blanketed with nitrogen

and covered immediately after sample collection to minimize contamination by atmospheric carbon dioxide. This is especially necessary for the lower pH, nonbuffered solutions.

The Berea sandstone core (Lot 121682), courtesy of Exxon Production Research Company [27], is 44.7 cm long with a 6.48 cm^2 square cross-sectional area and a permeability of 0.5 μm^2. The epoxy encasement (GC Electronics) withstands prolonged immersion in the 50 ± 1°C water bath (National Appliance Company, 230A). Based on a tritiated-water study, the core pore volume is found to be 60.0 ± 0.6 cm^3 corresponding to a porosity of 0.21 and a solid density of 2.56/cm^3 in excellent agreement with accepted values for Berea [7,10,24]. X-ray diffraction analysis of the disaggregated rock shows that the clay fraction (i.e., particles < 2 μm in nominal diameter [6]) consists mainly of kaolinite with some mica and quartz [26]. SEM examination of the sandstone reveals that the kaolinite is mainly of the pore-lining texture [28].

All aqueous solutions are made with Barnstead singly distilled water which is subsequently vacuum degassed and filtered (0.45 μm Millipore). It has a conductivity < 10^{-6} S/cm and pH ~ 6. Chemicals are all analytic grade from either Fisher (NaOH) or Mallinckrodt (Na_2CO_3 and NaCl). Tritiated water (^3HOH) and radioactive carbon (^{14}C-tagged carbonate) are supplied by the New England Nuclear Company.

Effluent samples from the core are allowed to cool to ambient temperature (22°C) and are analyzed for hydroxyl ion concentration (Fisher glass microelectrode), sodium ion concentration (Orion combination electrode), and ^3HOH and ^{14}C (Packard Tri-Carb liquid scintillation counter). Sodium concentrations permit assessment of the predicted intermediate plateau (see Fig. 2) while radioactive carbon levels test Eqn. (11). When tagged water

and carbonate are employed simultaneously, the tritiated water must have at least twice the count level of the ^{14}C to minimize interference [26].

A large number of NaOH displacements were conducted over the pH range from 11 to 13 in 1 and 2 w/o NaCl solutions. Frontal analysis [8,12,14,29] permits construction of the sodium/hydrogen ion-exchange isotherm, as shown by the closed and open circles in Fig. 4. Since hydroxide ion concentration does not have a zero value, the exchange isotherm must be measured relative to a reference uptake, n^o_{Na} , [14] or from Eqn. (7):

$$(n_{Na} - n^o_{Na})/n_{max} = \frac{K_I C_{Na} C_{OH}}{1 + K_I C_{Na} C_{OH}} - \frac{K_I C^o_{Na} C^o_{OH}}{1 + K_I C^o_{Na} C^o_{OH}} \quad , \qquad (20)$$

where the superscript o indicates the reference state. For convenience, we chose the brine preflush state of pH = 9.4 in 1 w/o NaCl to be the reference. The meaning of NaOH uptake in Fig. 4 is $(n_{Na} - n^o_{Na})$, where n^o_{Na} is the sodium loading at pH = 9.4 in 1 w/o NaCl. Choice of a particular reference state is irrelevant to the buffer chromatography calculations because only differences in n_{Na} appear. However, the reference state must be recognized and Eqn. (20) used when the parameters K_I and n_{max} are obtained from the experimental data.

A solid line in Fig. 4 gives a fit of Eqn. (20) to the 1 w/o NaCl background isotherm. The fit accentuates pH values near 11.5 since the Na_2CO_3 buffer experiments operate in this region. K_I is found to be $10^{3.3}$ N^{-2} and n_{max} = 0.18 mequiv/100g of solid rock. The dashed line in Fig. 4 is predicted using these parameters and Eqn. (20) for the 2 w/o NaCl background brine. Agreement is acceptable.

Since the same Berea core is repeatedly exposed to alkali, there is concern that the sand is eventually altered by mineral dissolution. Because of the relatively short core length and high flow rates employed, very little reaction loss is found. The effluent pH almost (but not quite) matches the inlet value (see Figs. 5-9 to follow) and no dissolved silica was detected using AAS. Continuing pressure-drop measurements (Validyne transducer) and tagged-water pore-volume determinations demonstrate no change of permeability or porosity. Most importantly, the sodium/hydrogen exchange isotherm remained the same (some of the points in Fig. 4 were repeated late in the experimental program). We conclude that no important chemical or physical alteration of the core occurred.

More details on the experimental apparatus and procedures are available elsewhere [26].

RESULTS

Figs. 5-7 highlight the experimental and theoretical results for injecting 0.1, 0.5, and 1.0 w/o (pH_i = 10.7, 11.4, and 11.6) Na_2CO_3 solutions in 1 w/o NaCl, respectively, into the Berea sandstone. Concentration histories are displayed for ^3HOH, ^{14}C, Na^+, and OH^-, on dimensionless scales of $(C_L - C_o)/(C_i - C_o)$ versus throughput PV, where C_L is the species effluent concentration, and C_o and C_i are their initial and inlet values. Open and filled symbols reflect the experimental data, while solid and various dashed lines give the buffer chromatography calculations. We stress that in the model predictions no adjustable constants are available. The small discrepancy between the inlet and the steady outlet hydroxide concentrations is due to mineral dissolution, as discussed previously.

In all figures elution of the total carbon (^{14}C) exactly parallels the labelled water (^{3}HOH). Strong confirmation is thus seen for the unit-velocity propagation of the total carbon wave according to Eqns. (9) and (11). Exiting sodium ion concentrations clearly demonstrate an intermediate-plateau region whose duration shrinks with increasing buffer capacity. Equivalently, the mean breakthrough times of the alkali diminish for the more concentrated carbonate solutions.

Detailed comparison between the predicted and experimental sodium and hydroxide histories shows some discrepancies which are slightly outside the estimated error limits. The largest deviation in the mean alkali breakthrough time is 8% as evidenced with the 0.1 w/o carbonate buffer. Since the theoretical predictions in these figures are a priori, such deviations seem acceptable.

Fig. 8 permits closer scrutiny of the hydroxide history for the 0.1 w/o carbonate buffer. Here pH_L appears as the ordinate. The slight drop in pH predicted for the intermediate plateau is verified.

Figs. 5-8 evidence considerable spreading of the sodium and hydroxide effluent concentrations, not accounted for in the proposed theory. Significant dispersion for these two ions is possibly caused by an internal diffusion resistance retarding access to the mineral base exchange sites [26,28]. The present buffer chromatography theory attempts only to establish the mean concentration velocities about which any dispersion is centered. We assert that the theoretical analysis correctly reflects all qualitative trends and provides acceptable quantitative agreement.

Cursory examination of Eqn. (1) suggests that sodium/hydrogen ion-exchange lag may be overcome by increasing either the flooding solution hydroxide level or the sodium level. It might be argued that raising the

brine concentration in a dilute caustic flood is as effective as a buffer displacement, as long as the sodium and hydroxide concentration are equivalent. Fig. 9 reveals that this reasoning is oversimplified.

This figure gives the experimental data and theoretical predictions for injection of a 2.08 w/o NaCl, 0.02 w/o NaOH (pH_I = 11.7) solution into the Berea sandstone. These sodium and hydroxide concentrations are equivalent to those for injection of the 1 w/o Na_2CO_3, 1 w/o NaCl solution in Fig. 7. Striking differences are found. The intermediate-plateau sodium level is much higher, and the alkali breakthrough time is much longer (i.e., 3.4 PV versus 1.4 PV) for the caustic. Clearly, the buffer chemistry of Eqns. (2) and (4) permits faster chromatographic transport of the alkali. Our theoretical analysis correctly predicts the observed results giving further weight to its validity.

RAMIFICATIONS

In Figs. 10 and 11, alkali breakthrough is graphed against solution pH. Fig. 10 summarizes our experimental efforts. Fig. 11 is taken from the recent work of Burk [4] also with a Berea core. Solid lines are fit to obtain the ion-exchange parameters K_I and n_{max}, while dashed lines give the chromatography theory predictions. Fig. 10 provides a much stronger validation of the theory because only two experimental NaOH histories were determined by Burk so that K_I and n_{max} in Fig. 11 are not unique.

Figs. 10 and 11 accentuate the main finding of this paper: buffered alkaline solutions provide a major improvement in alkali propagation rate through Berea sandstone. In more argillaceous sands even more improvement can be expected. Relative to NaOH improvement is larger for Na_2CO_3 versus Na_4SiO_4 because carbonate buffers in a lower pH range. From a mineral reaction

viewpoint, use of lower pH flooding solutions appears advantageous, subject to the alkali concentration being sufficient to activate the acid surfactant precursors. Thus, lower pH, highly buffered alkaline solutions hold the promise of surviving under field application.

CONCLUSIONS

We make the following conclusions:

1. Dynamic column experiments demonstrate that buffered alkali provides a dramatic improvement in chromatographic propagation speed over unbuffered alkali in base exchanging reservoir sands.
2. A theoretical chromatographic model quantifies the ion-exchange transport behavior of buffered alkali, such as Na_2CO_3, and Na_4SiO_4, in linear porous media exhibiting mineral surface sodium/hydrogen ion exchange.
3. The theoretical model agrees semi-quantitatively with the experimental column results for the concentration histories developed upon buffered alkaline flooding. No adjustable constants are used in the comparison. The predicted intermediate plateau is confirmed.

NOMENCLATURE

C_i = bulk solution concentration of species i, kmol/m^3.

f = function defined in Eqn. (14).

K_1 = equilibrium constant for carbonate hydrolysis in Eqn. (2), kmol/m^3.

K_2 = equilibrium constant for bicarbonate hydrolysis in Eqn. (4), kmol/dm^3.

K_3 = equilibrium constant for divalent silicate hydrolysis in Eqn. (3), kmol/m^3.

K_4 = equilibrium constant for monovalent silicate hydrolysis in Eqn. (19), kmol/m^3.

K_I = sodium/hydrogen ion-exchange equilibrium constant in Eqn. (1), $(m^3/kmol)^2$.

K_w = equilibrium constant for water dissociation in Eqn. (5), $(kmol/m^3)^2$.

L = column length, m.

$\bar{M}$ = mineral base exchange site.

n_{Na} = amount of sodium ion exchanged on solid mineral surface, kmol/kg.

n_{max} = hydrogen ion-exchange capacity, kmol/kg.

t = time, s.

$\tilde{t}$ = $ut/\phi L$, reduced time or fluid throughput pore volumes, PV.

T = temperature, K.

u = superficial velocity, m/s.

v = u/ϕ, interstitial velocity, m/s.

z = axial column distance, m.

$\tilde{z}$ = z/L, reduced column axial distance.

Greek Symbols

ϕ = porosity.

ρ_s = solid density, kg/m^3.

Subscripts

b = breakthrough

be = experimental breakthrough

i = inlet or species

L = effluent

o = initial or presaturation

Superscripts

o = reference

I = Region I

II = Region II

III = Region III

Other Symbols

[ ] = bulk molar concentration, $kmol/m^3$.

ACKNOWLEDGEMENTS

This work was performed with partial financial support of the Department of Energy to the Lawrence Berkeley Laboratory of the University of California under contract DE-AC03-76SF00098. JAJ acknowledges aid from the Stauffer Chemical Company.

REFERENCES

1. Johnson, C.E., Jr.: "Status of Caustic and Emulsion Methods," J. Pet. Tech. (Jan. 1970) 85-92.

2. Nelson, R.C., Lawson, J.B., Thigpen, D.R., and Stegemeier, G.L.: "Cosurfactant-Enhanced Alkaline Flooding," SPE/DOE 12672, presented at the 4th SPE/DOE Symposium on Enhanced Oil Recovery, Tulsa, OK, April 15-18, 1983.

3. Radke, C.J.: "Additives for Alkaline Recovery of Heavy Oil," Proceedings of the 1982 Heavy Oil Symposium, Department of Energy (July 1982) 2-19.

4. Burk, J.H.: "Comparison of Sodium Carbonate, Sodium Hydroxide, and Sodium Orthosilicate for EOR," SPE 12039, presented at the 58th Annual Fall Technical Conference of SPE, San Francisco, CA, October 5-8, 1983.

5. Ehrlich, R., and Wygal, R.J., Jr.: "Interrelation of Crude Oil and Rock Properties with the Recovery of Oil by Caustic Waterflooding," Soc. Pet. Eng. J. (Aug. 1977) 263-270.

6. Somerton, W.H., and Radke, C.J.: "Role of Clays in the Enhanced Recovery of Petroleum," J. Pet. Tech. (March, 1983) 643-654.

7. Sydansk, R.D.: "Elevated-Temperature Caustic/Sandstone Interaction: Implications for Improving Oil Recovery," Soc. Pet. Eng. J. (Aug. 1982) 453-462.

8. Bunge, A.L., and Radke, C.J.: "Migration of Alkaline Pulses in Reservoir Sands," Soc. Pet. Eng. J. (Dec. 1982) 998-1012.

9. Southwick, J.G.: "Solubility of Silica in Alkaline Solutions: Implications for Alkaline Flooding," SPE 12771, presented at the 1984 California Regional SPE Meeting, Long Beach, CA, April 11-13, 1984.

10. Krumrine, P.H., and Falcone, J.S., Jr.: "Rock Dissolution and Consumption Phenomena in an Alkaline Recovery Ssytem," SPE/DOE 12670, presented at the 4th SPE/DOE Symposium on Enhanced Oil Recovery, Tulsa, OK, April 15-18, 1984.

11. Mohnot, S.M., Bae, J.H., and Foley, W.L.: "A Study of Mineral-Alkali Reactions," SPE 13032, presented at the 59th Annual Fall Technical Conference of SPE, Houston, TX, September 16-19, 1984.

12. deZabala, E.F., Vislocky, J.M., Rubin, E., and Radke, C.J.: "A Chemical Theory for Linear Alkaline Waterflooding, " Soc. Pet. Eng. J. (April, 1982) 245-258.

13. Novosad, Z., and Novosad, J.: "The Effect of Hydrogen Ion Exchange on Alkalinity Loss in Alkaline Flooding," paper SPE 10605, presented at the 6th SPE Intl. Symposium on Oilfield and Geothermal Chemistry, Dallas, TX, Jan. 25-27, 1982.

14. Bunge, A.L., and Radke, C.J.: "The Origin of Reversible Hydroxide Uptake on Reservoir Rock," paper SPE 11790, presented at the International Symposium on Oilfield and Geothermal Chemistry, Denver, CO, June 1-3, 1983, Soc. Pet. Eng. J. to appear (December, 1985).

15. Ting, D.C.: "The Kinetics of Alkaline Consumption of Silicate Minerals," M.S. Thesis, University of California, Berkeley, (1985) in preparation.

16. Thornton, S.D., and Radke, C.J.: "Dissolution and Condensation Kinetics of Silica in Alkaline Solution," SPE 13601, presented at the California Regional Meeting of SPE, Bakersfield, CA, March 27-29, 1985.

17. _____: "Handbook of Chemistry and Physics," CRC Press, 56th Ed., 1976.

18. Ingri, N.: "Equilibrium Studies of Polyanions, IV. Silicate Ions in NaCl Medium," Acta Chem. Scand. (1959) 13(4), 758-775.

19. Helferrich, F.G., and Klein, G.: "Multicomponent Chromatography: Theory of Interference," Marcel Dekker, New York, 1970.

20. Klein, G., Norem, N.J., and Vermeulen, T.: "Studies on the Behavior of Carbonic Acid and its Salts in Fixed Beds of Weak-Acid Ion Exchangers," Ion-Exchange Symposium Proceedings, Bhavnagar, India (February, 1978) 119-130.

21. Sherwood, T.K., Pigford, R.L., and Wilke, C.R.: "Mass Transfer," Chapter 10, McGraw-Hill, New York, 1975.

22. Aris, R., and Amundson, N.R., "Mathematical Methods in Chemical Engineering," Vol. 2, Prentice-Hall, New Jersey, 1973.

23. Helferrich, F.G.: "Theory of Multicomponent, Multiphase Displacement in Porous Media," Soc. Pet. Eng. J. (February, 1981) 51-62.

24. Pope, G.A., Lake, L.W., and Helferrich, F.G.: "Cation Exchange in Chemical Flooding: Part 1 - Basic Theory without Dispersion," Soc. Pet. Eng. J. (December, 1978) 418-434.

25. Hiester, N.K., Klein, G., and Vermeulen, T.: "Adsorption and Ion Exchange," Chemical Engineers Handbook, 4th Edition, J.H. Perry, ed., McGraw-Hill (1963) Section 16, 1-39.

26. Jensen, J.A.: "Chromatographic Transport of Alkaline Buffers in Underground Porous Media," M.S. Thesis, University of California, Berkeley, 1985.

27. Seright, R., Exxon Production Research Company, Houston, TX, personal communication, 1984.

28. Jensen, J.A., Gillis, J.V., and Radke, C.J.: "Dispersion Attendant Sodium/Hydrogen Ion Exchange in Reservoir Sands," Soc. Pet. Eng. J., submitted, 1985.

29. Wang, H.L., Duda, J.L., and Radke, C.J.: "Solution Adsorption from Liquid Chromatography, " J. Coll. Int. Sci. (1978) 66(1), 153-165.

APPENDIX: Functionality between Hydroxide and the Independent Species

Eqns. (2), (4), and (5), in their mass-action forms, and Eqns. (6) and (10) of the text combine to establish f of Eqn. (14). Let $\hat{C}_{OH} = C_{OH}/K_1$ define a reduced hydroxide concentration. Then we find that

$$\hat{C}_{OH}^4 + [1 + 2C_{TC}/K_1 - (C_{Na} - C_{Cl})/K_1]\, \hat{C}_{OH}^3$$

$$+ (K_2/K_1)\, [1 + C_{TC}/K_2 - K_w/(K_1K_2) - (C_{Na} - C_{Cl})/K_2]\, \hat{C}_{OH}^2$$

$$- (K_w/K_1)^2\, [1 + (C_{Na} - C_{Cl})\, K_2/K_w]\, \hat{C}_{OH} - K_2K_w/K_1^3 = 0 \,. \qquad \text{(A1)}$$

Given C_{Na}, C_{Cl}, and C_{TC}, Eqn. (A1) is solved by trial-and-error to yield $\hat{C}_{OH}$ [26]. This process is represented schematically by Eqn. (14).

Table 1 Equilibrium Constants at 25°C

Reaction Eqn.	pK	Ref.
(2)	$pK_1 = 3.75$	[17]
(3)	$pK_3 = 1.0$	[8]
(4)	$pK_2 = 7.63$	[17]
(5)	$pK_w = 14$	[17]
(19)	$pK_4 = 4.3$	[8]

FIGURE CAPTIONS

Figure 1. Characteristic $\tilde{z} - \tilde{t}$ diagram for the alkaline buffer chromatography theory. Three concentration regions are shown, and two wave velocities are identified.

Figure 2. Calculated concentration histories for continuous injection of a 1 w/o Na_2CO_3 (pH_I = 11.6), 1 w/o NaCl buffer solution. An alkali breakthrough time of $\tilde{t}_b$ = 1.74 PV is predicted.

Figure 3. Calculated concentration histories for continuous injection of a 0.016 w/o NaOH (pH_I = 11.6), 1 w/o NaCl caustic solution. An alkali breakthrough time of $\tilde{t}_b$ = 12.4 PV is predicted.

Figure 4 Relative sodium/hydrogen ion-exchange isotherm for Berea sandstone or ($n_{Na} - n^o_{Na}$) versus hydroxide concentration in 1 and 2 w/o NaCl background solutions at 50°C. The ion-exchange parameters K_I and n_{max} are fit only with the 1 w/o NaCl data. Error bars are shown.

Figure 5 Comparison of experimental and theoretical concentration histories for injection of 0.1 w/o Na_2CO_3, 1 w/o NaCl into Berea sandstone at 50°C. The experimental breakthrough time of the alkali is $\tilde{t}_{be}$ = 2.06 . Typical error bars are shown.

Figure 6 Comparison of experimental and theoretical concentration histories for injection of 0.5 w/o Na_2CO_3, 1 w/o NaCl into Berea sandstone at 50°C. The experimental breakthrough time of the alkali is $\tilde{t}_{be}$ = 1.53 PV . Typical error bars are shown.

Figure 7 Comparison of experimental and theoretical concentration histories for injection of 1 w/o Na_2CO_3, 1 w/o NaCl into Berea sandstone at 50°C. The experimental breakthrough time of the alkali is $\tilde{t}_{be}$ = 1.38 PV. Typical error bars are shown.

Figure 8 Detailed comparison of the experimental and theoretical hydroxide history on a pH scale for injection of 0.1 w/o Na_2CO_3, 1 w/o NaCl into Berea sandstone at 50°C. The experimental breakthrough time of the alkali is $\tilde{t}_{be}$ = 2.06 PV .

Figure 9 Comparison of experimental and theoretical concentration histories for injection of 0.02 w/o NaOH, 2.08 w/o NaCl into Berea sandstone at 50°C. The experimental breakthrough time of the alkali is $\tilde{t}_{be}$ = 3.4 PV . Typical error bars are shown.

Figure 10 Comparison of experimental and theoretical alkali breakthrough times of NaOH and Na_2CO_3 as a function of injection pH. Typical error bars are shown.

Figure 11 Comparison of experimental and theoretical alkali breakthrough times for NaOH, Na_4SiO_4, and Na_2CO_3 as a function of injection pH. Experimental data are from Burk [4].

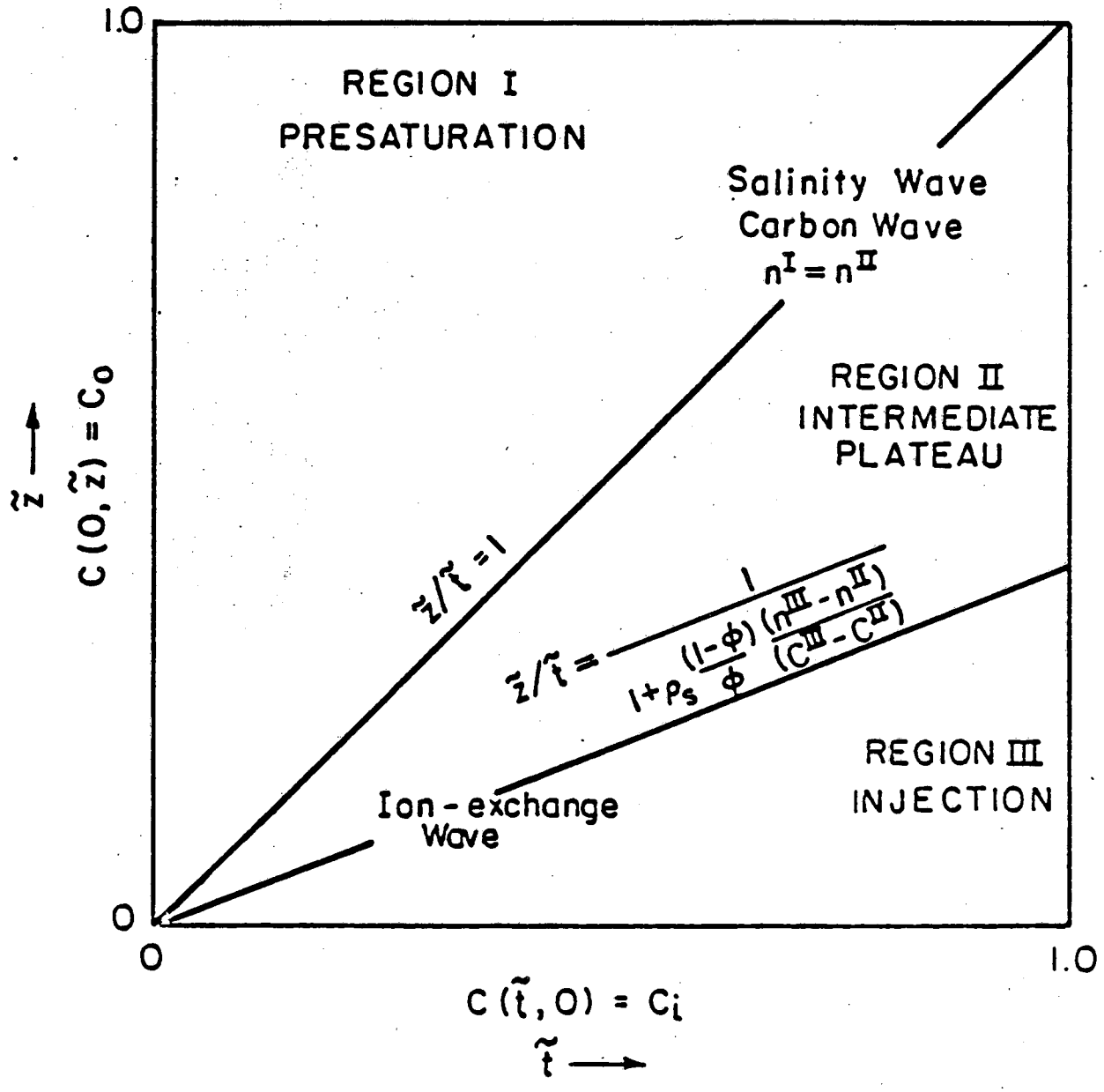
1.0
REGION I
PRESATURATION
Salinity Wave
Carbon Wave
$n^I = n^{II}$
REGION II
INTERMEDIATE
PLATEAU
$\tilde{z}/\tilde{t} = 1$
$\tilde{z}/\tilde{t} = \frac{1}{1+\rho_s \frac{(1-\phi)}{\phi} \frac{(n^{III}-n^{II})}{(C^{III}-C^{II})}}$
REGION III
INJECTION
Ion-exchange
Wave
$\tilde{z} \longrightarrow$
$C(0,\tilde{z}) = C_0$
0
0
1.0
$C(\tilde{t},0) = C_i$
$\tilde{t} \longrightarrow$

Figure 1.

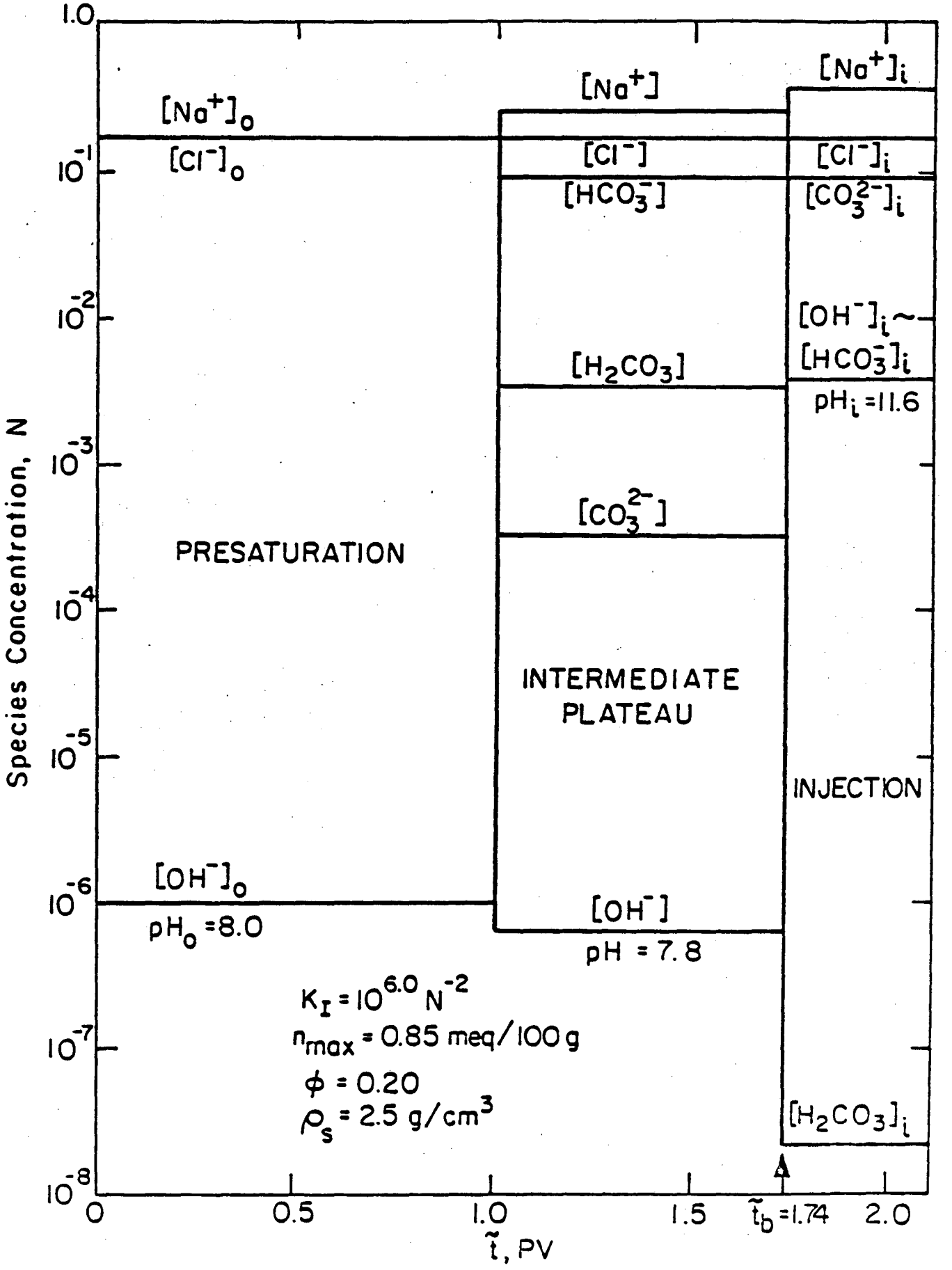
1.0
10^{-1}
10^{-2}
10^{-3}
10^{-4}
10^{-5}
10^{-6}
10^{-7}
10^{-8}
Species Concentration, N
$[Na^+]_o$
$[Cl^-]_o$
$[OH^-]_o$
$pH_o = 8.0$
PRESATURATION
$[Na^+]$
$[Cl^-]$
$[HCO_3^-]$
$[H_2CO_3]$
$[CO_3^{2-}]$
INTERMEDIATE PLATEAU
$[OH^-]$
pH = 7.8
$[Na^+]_i$
$[Cl^-]_i$
$[CO_3^{2-}]_i$
$[OH^-]_i \sim$
$[HCO_3^-]_i$
$pH_i = 11.6$
INJECTION
$[H_2CO_3]_i$
$K_I = 10^{6.0}\ N^{-2}$
$n_{max} = 0.85$ meq/100 g
$\phi = 0.20$
$\rho_s = 2.5$ g/cm^3
0
0.5
1.0
1.5
$\tilde{t}_b = 1.74$
2.0
$\tilde{t}$, PV

Figure 2.

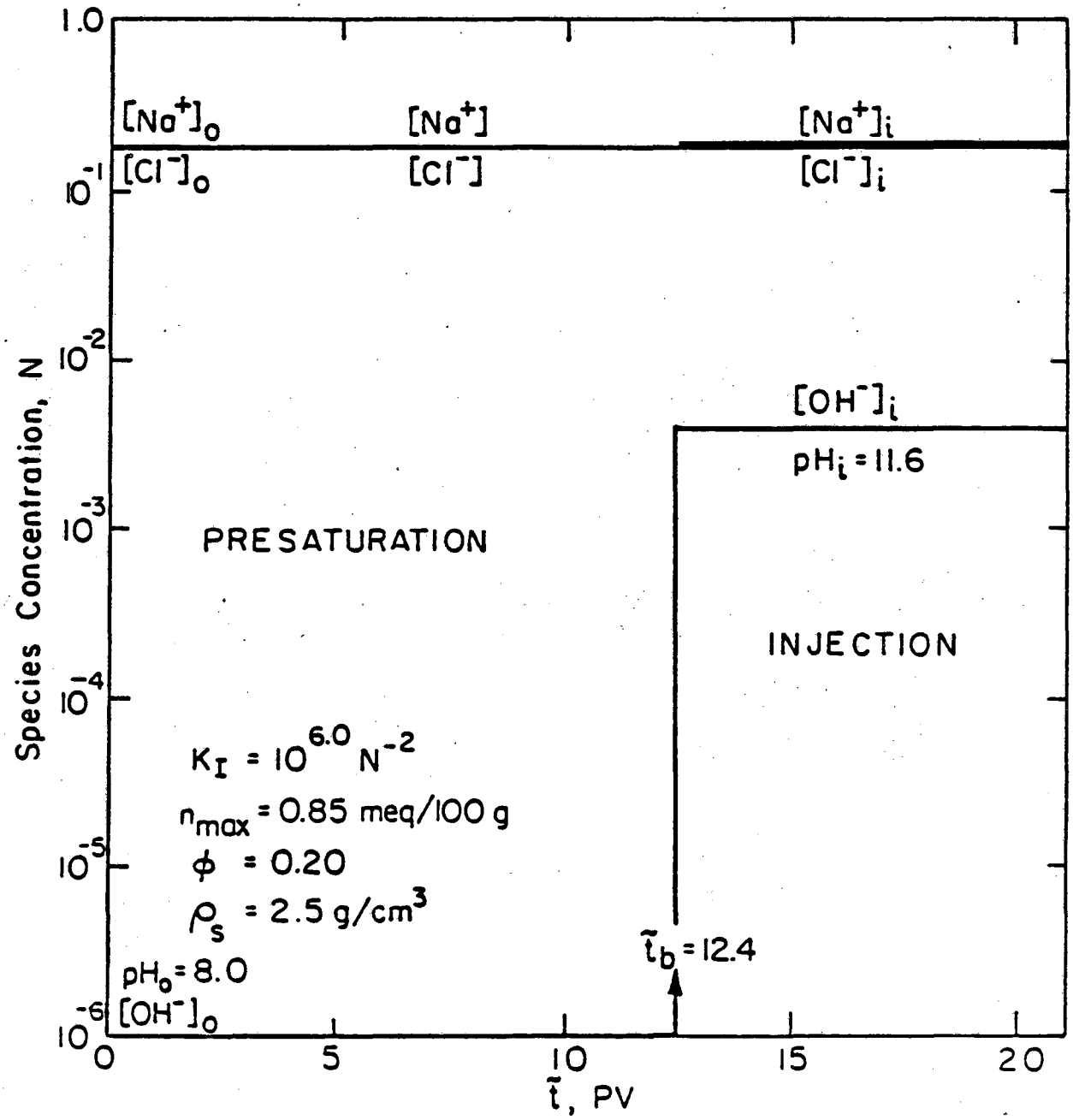
1.0
$[Na^+]_o$
$[Cl^-]_o$
$[Na^+]$
$[Cl^-]$
$[Na^+]_i$
$[Cl^-]_i$
10^{-1}
10^{-2}
$[OH^-]_i$
$pH_i = 11.6$
10^{-3}
PRESATURATION
INJECTION
10^{-4}
$K_I = 10^{6.0}\ N^{-2}$
$n_{max} = 0.85$ meq/100 g
$\phi = 0.20$
$\rho_s = 2.5$ g/cm^3
10^{-5}
$\tilde{t}_b = 12.4$
$pH_o = 8.0$
$[OH^-]_o$
10^{-6}
Species Concentration, N
0
5
10
15
20
$\tilde{t}$, PV

Figure 3.

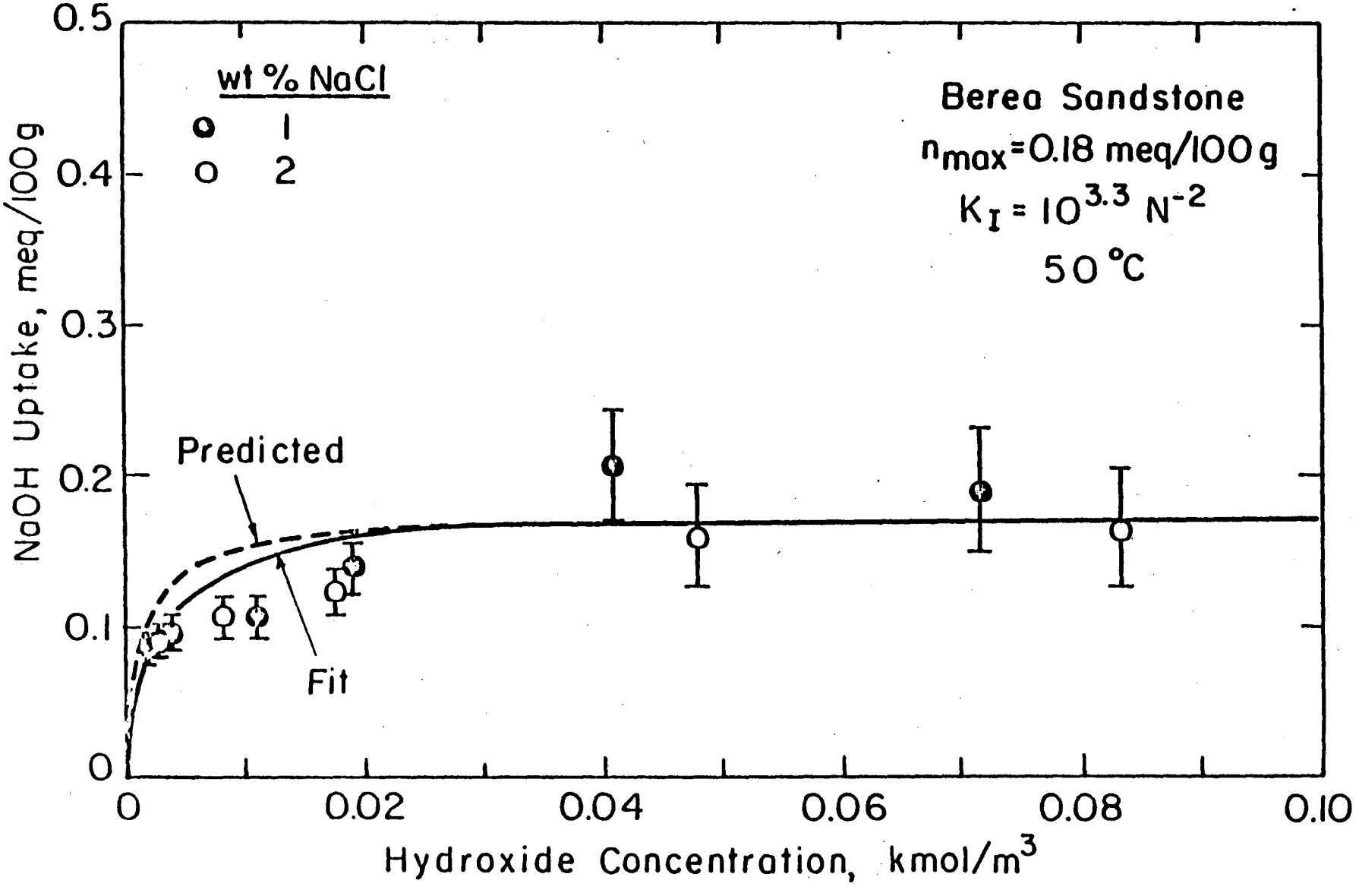
wt % NaCl
1
2
Berea Sandstone
n_{max}=0.18 meq/100g
$K_I = 10^{3.3}\ N^{-2}$
50 °C
Predicted
Fit
NaOH Uptake, meq/100g
Hydroxide Concentration, kmol/m^3
0.5
0.4
0.3
0.2
0.1
0
0.02
0.04
0.06
0.08
0.10

Figure 4.

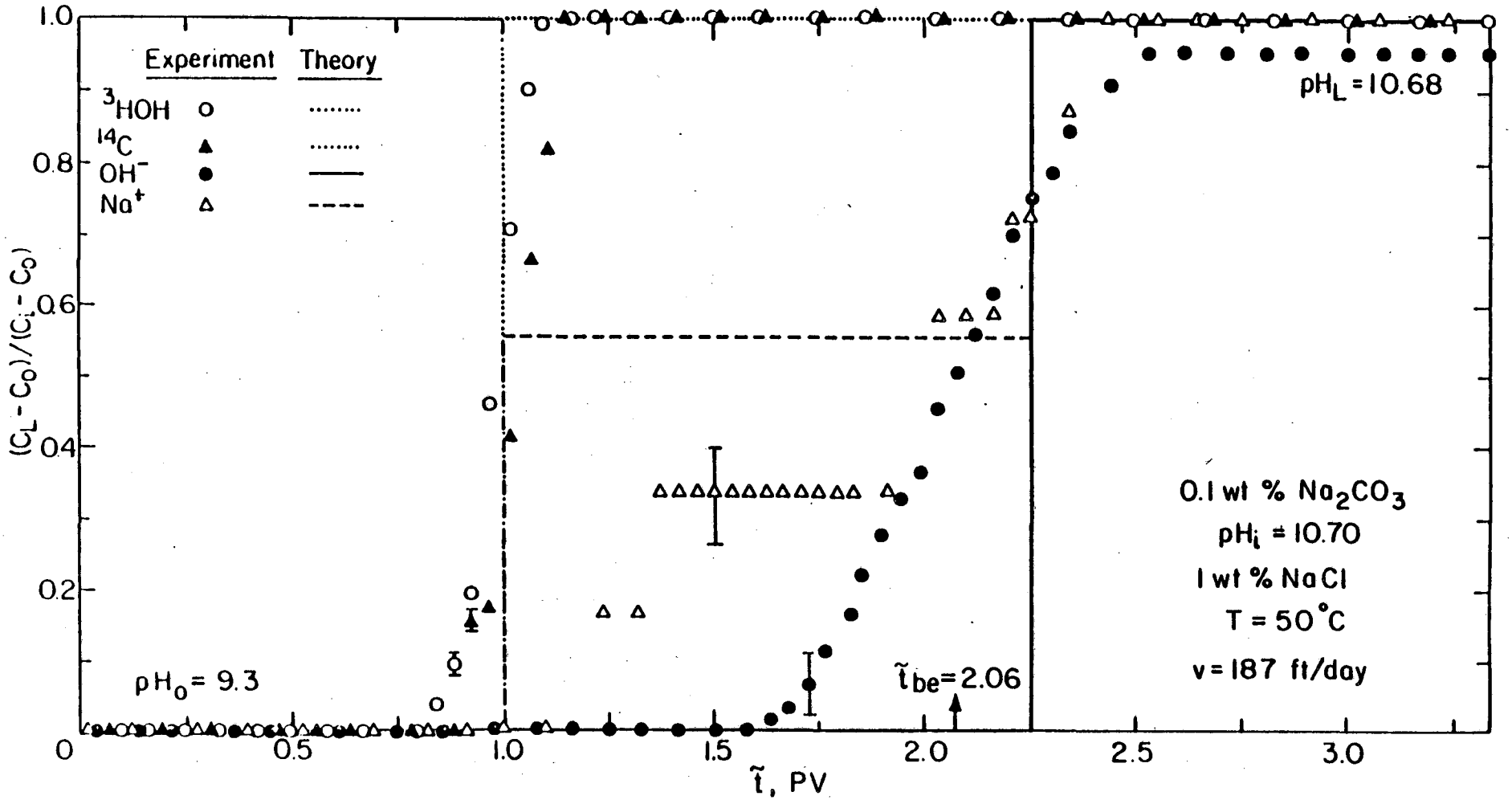
Experiment
Theory
^{3}HOH
^{14}C
OH$^-$
Na$^+$
pH$_L$ = 10.68
0.1 wt % Na$_2$CO$_3$
pH$_i$ = 10.70
1 wt % NaCl
T = 50°C
v = 187 ft/day
pH$_0$ = 9.3
$\tilde{t}_{be}$ = 2.06
$(C_L - C_0)/(C_i - C_0)$
$\tilde{t}$, PV
0
0.2
0.4
0.6
0.8
1.0
0.5
1.0
1.5
2.0
2.5
3.0

Figure 5.

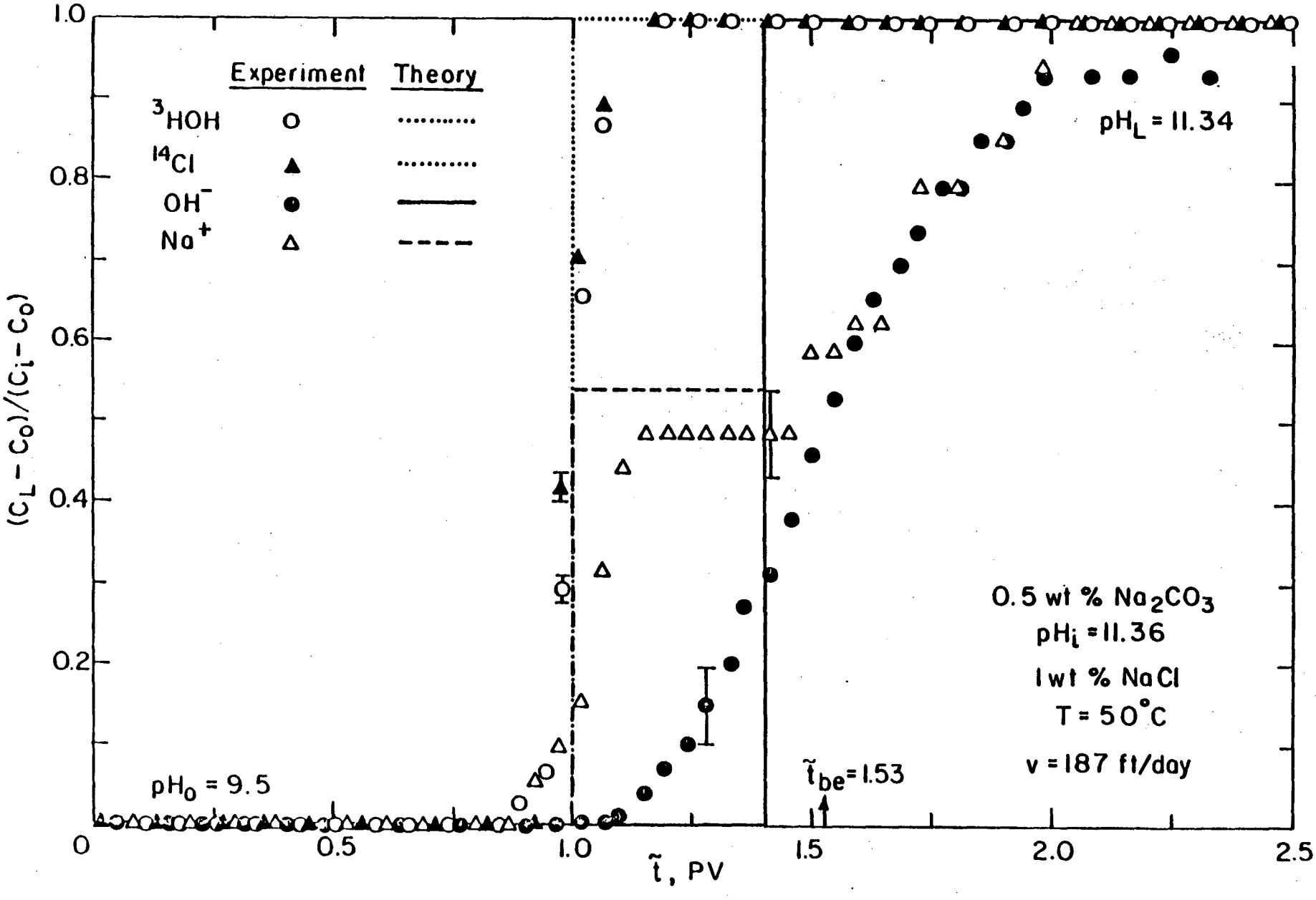
Experiment
Theory
^{3}HOH
^{14}Cl
OH^-
Na^+
pH_L = 11.34
0.5 wt % Na_2CO_3
pH_i = 11.36
1 wt % NaCl
T = 50°C
v = 187 ft/day
pH_0 = 9.5
$\tilde{t}_{be}$ = 1.53
$(C_L - C_0)/(C_i - C_0)$
$\tilde{t}$, PV
0
0.2
0.4
0.6
0.8
1.0
0.5
1.0
1.5
2.0
2.5

Figure 6.

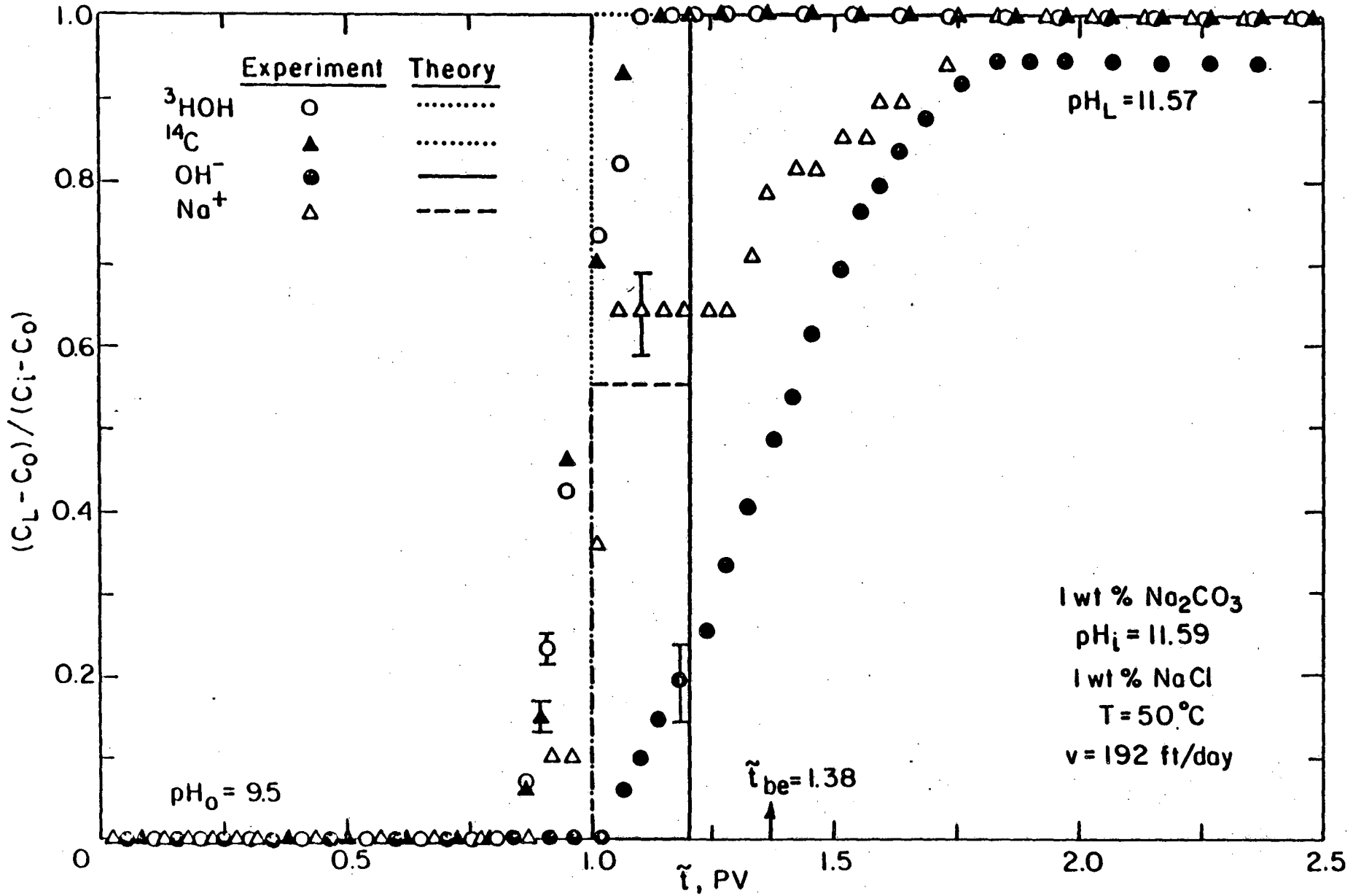
Experiment
Theory
^3HOH
^{14}C
OH^-
Na^+
$pH_L = 11.57$
1 wt % Na_2CO_3
$pH_i = 11.59$
1 wt % NaCl
T = 50 °C
v = 192 ft/day
$pH_0 = 9.5$
$\tilde{t}_{be} = 1.38$
$(C_L - C_0)/(C_i - C_0)$
$\tilde{t}$, PV
0
0.2
0.4
0.6
0.8
1.0
0.5
1.0
1.5
2.0
2.5

Figure 7.

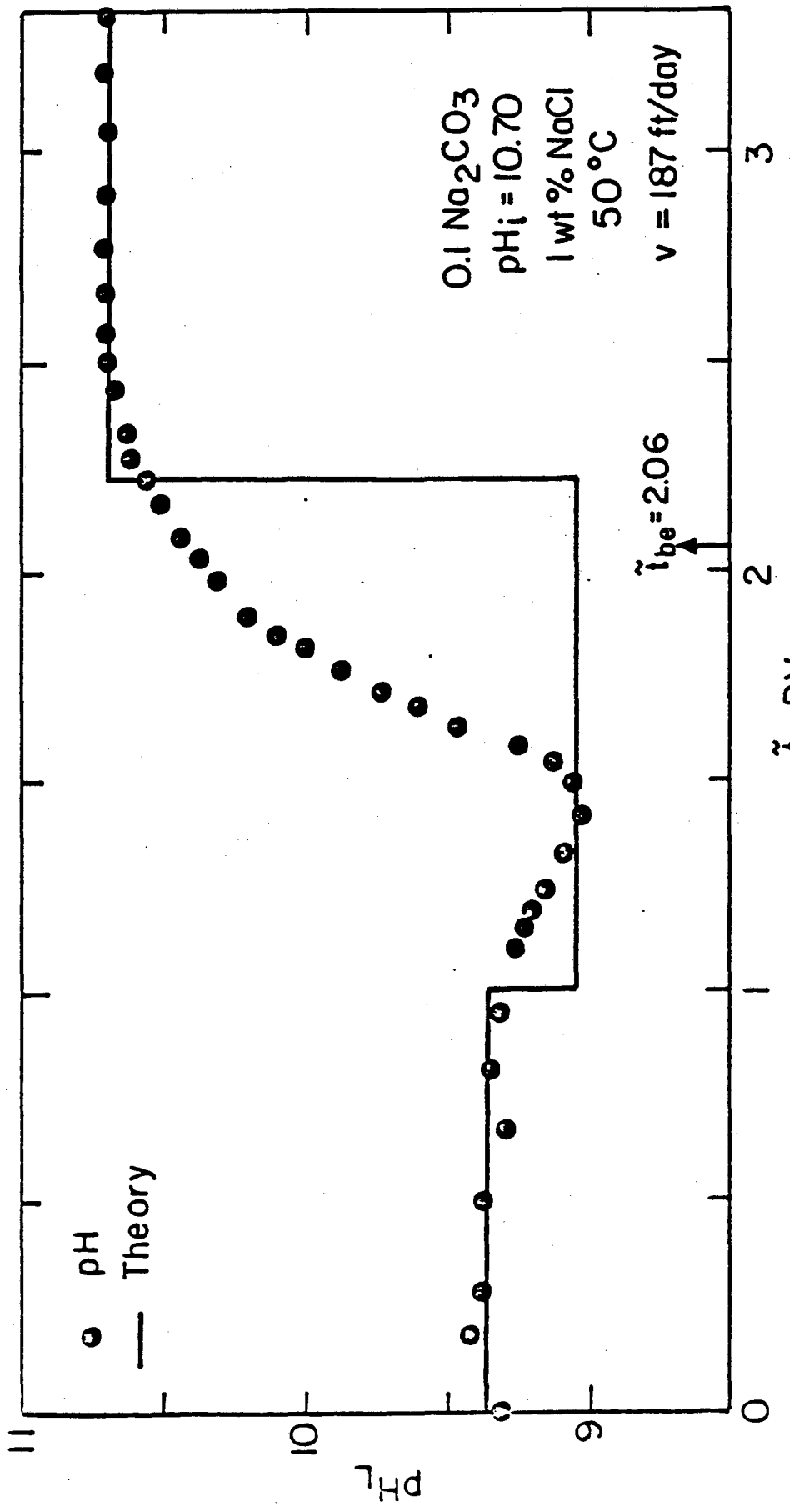
0.1 Na_2CO_3
pHi = 10.70
1 wt % NaCl
50 °C
v = 187 ft/day
$\tilde{t}_{be}$=2.06
pH
Theory
pH_L
$\tilde{t}$, PV
11
10
9
0
1
2
3

Figure 8.

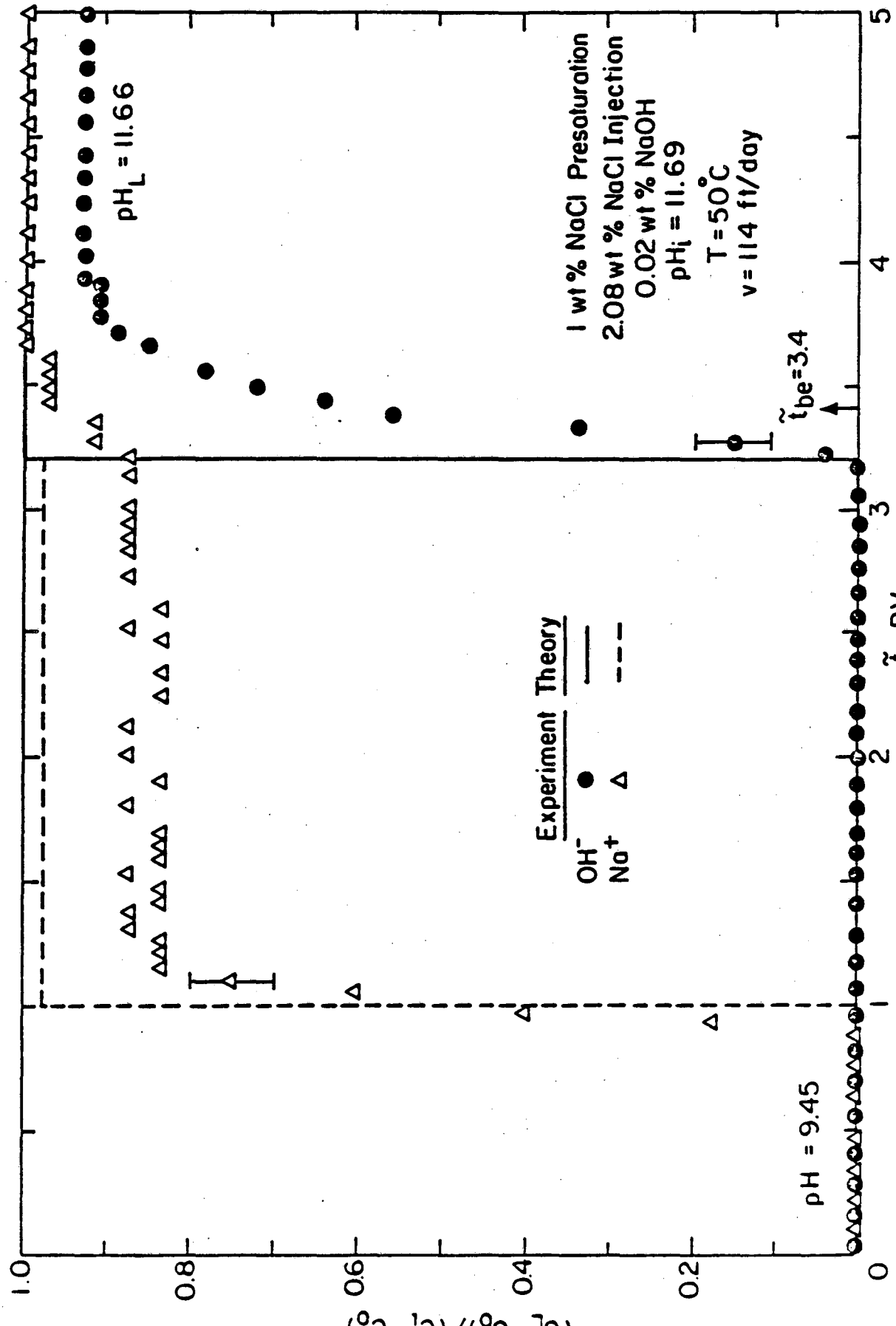
1 wt % NaCl Presaturation
2.08 wt % NaCl Injection
0.02 wt % NaOH
pH$_i$ = 11.69
T = 50°C
v = 114 ft/day
pH$_L$ = 11.66
$\tilde{t}_{be}$=3.4
pH = 9.45
Experiment Theory
OH$^-$ ● ——
Na$^+$ △ ---
$(C_L - C_o)/(C_i - C_o)$
$\tilde{t}$, PV
0
0.2
0.4
0.6
0.8
1.0
1
2
3
4
5

Figure 9.

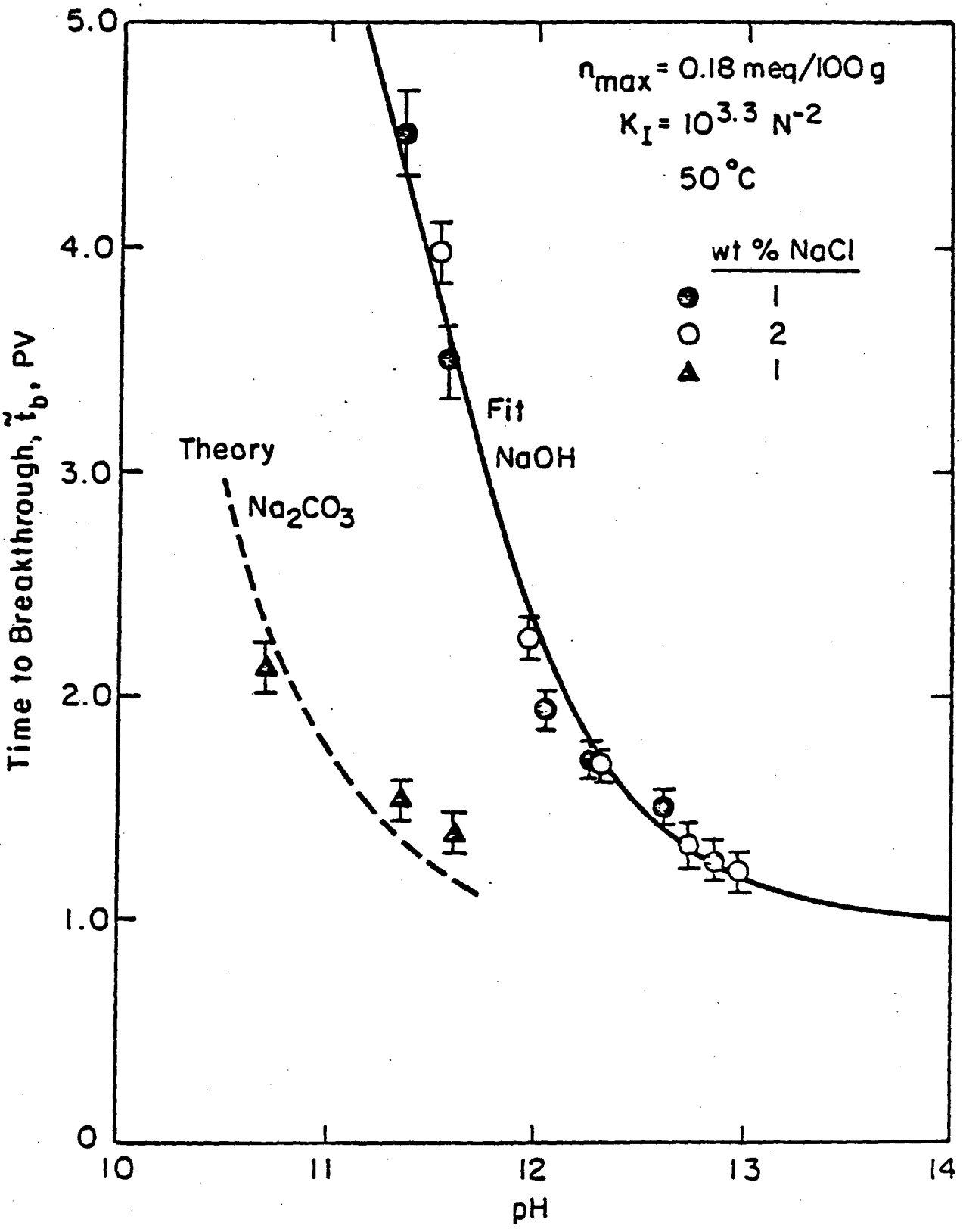
5.0
4.0
3.0
2.0
1.0
0
10
11
12
13
14
pH
Time to Breakthrough, $\tilde{t}_b$, PV
n_{max} = 0.18 meq/100 g
$K_I = 10^{3.3}$ N^{-2}
50 °C
wt % NaCl
1
2
1
Fit
NaOH
Theory
Na_2CO_3

Figure 10.

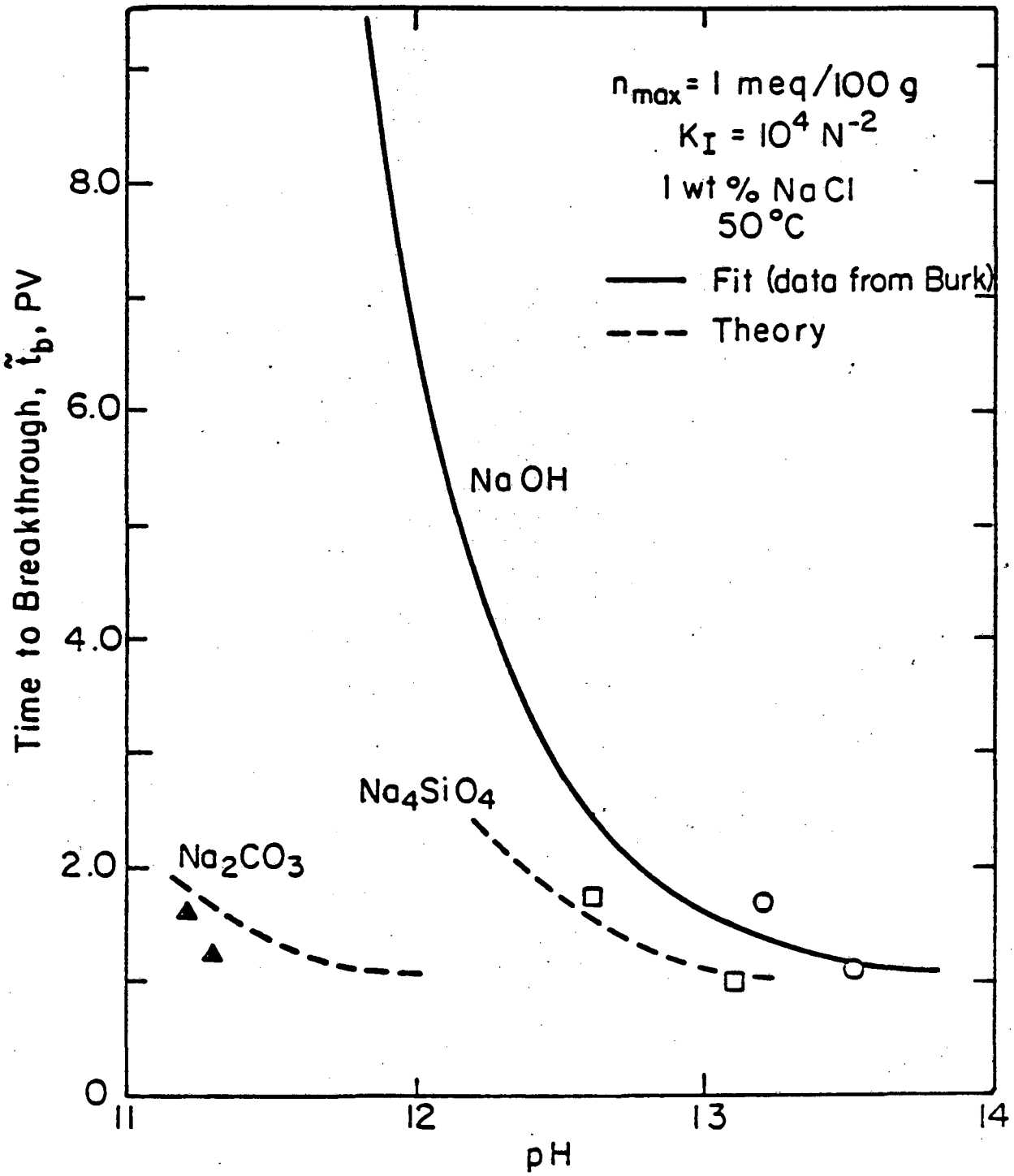
n_{max} = 1 meq/100 g
$K_I = 10^4\ N^{-2}$
1 wt % NaCl
50°C
Fit (data from Burk)
Theory
NaOH
Na_4SiO_4
Na_2CO_3
Time to Breakthrough, $\tilde{t}_b$, PV
pH
0
2.0
4.0
6.0
8.0
11
12
13
14

Figure 11.

TECHNICAL INFORMATION DEPARTMENT
LAWRENCE BERKELEY LABORATORY
UNIVERSITY OF CALIFORNIA
BERKELEY, CALIFORNIA 94720